# Evaluation of spatter particles, metal vapour jets, and depressions considering influence of laser incident angle on melt pool behaviour

**Kotaro Tsubouchi** ( k.tsubouchi@stu.kanazawa-u.ac.jp )
Kanazawa University: Kanazawa Daigaku
**Tatsuaki Furumoto**
Kana-zawa University
**Mitsugu Yamaguchi**
Kana-zawa University
**Atsushi Ezura**
Kana-zawa University
**Shinnosuke Yamada**
Daido Steel Co., Ltd., Higashisakura 1-chome 1-10
**Mototsugu Osaki**
Daido Steel Co., Ltd., Higashisakura 1-chome 1-10
**Kenji Sugiyama**
Daido Steel Co., Ltd., Higashisakura 1-chome 1-10

**Research Article**

**Keywords:** Additive manufacturing, Powder bed fusion, In-process monitoring, Laser incident angle, Melt pool, Spatter particle

**Posted Date:** October 27th, 2021

**DOI:** https://doi.org/10.21203/rs.3.rs-1017930/v1



**Version of Record:** A version of this preprint was published at The International Journal of Advanced Manufacturing Technology on February 15th, 2022. See the published version at https://doi.org/10.1007/s00170-022-08887-w.

# Evaluation of spatter particles, metal vapour jets, and depressions considering influence of laser incident angle on melt pool behaviour

Kotaro Tsubouchi[1] · Tatsuaki Furumoto[2] · Mitsugu Yamaguchi[2] · Atsushi Ezura[2] · Shinnosuke Yamada[3] · Mototsugu Osaki[3] · Kenji Sugiyama[3]

## Abstract

Building of practical parts involves the application of metal-based laser powder bed fusion using a laser beam (PBF-LB/M) owing to its high-precision manufacturing. However, the quality of the built parts obtained via the PBF-LB/M processes varies with the building conditions, and a thorough understanding of the building mechanism has not been achieved owing to the complex and interrelated process parameters involved. The incident angle of the laser beam, which changes on the platform during the laser beam scan owing to the designed three-dimensional data, is among the principal parameters that affects the building aspects. In this study, the melt pool in the single-track formation during the PBF-LB/M processes was visualised using a high-speed camera, and the influence of the laser incident angle on the ejection characteristics of spatter particles formed around the laser-irradiated area was investigated. Consequently, the spatter particles and metal vapour jet behaviour varied with the laser incident angle. There was a reduction in number of spatter particles owing to the origin of the incident direction being from behind the laser irradiation area. In addition, the laser incident angle also affected the melt pool morphology because of the depression in the melting. Furthermore, the burial depth of the pores varied with the laser incident angle, and is related to the depth of the depression during the melt pool formation.

**Keywords:** Additive manufacturing, Powder bed fusion, In-process monitoring, Laser incident angle, Melt pool, Spatter particle

## 1. Introduction

Additive manufacturing (AM) is defined as the "process of joining materials to fabricate objects from three-dimensional model data, usually layer upon layer, as opposed to subtractive manufacturing methodologies" as per the International Committee of the American Society for Testing Materials (ASTM) [1]. AM enables the building of topologically optimised and integrated composite parts according to digital 3D design data [2]. In particular, metal-based powder bed fusion using a laser beam (PBF-LB/M), which is one such AM technique, is expected to be applied to mechanical parts, such as a customised part with a lattice structure [3], a highly functional mould with conformal cooling channels [4], and a functionally graded part [5]. However, this technique suffers from the lack of fusion and the formation of defects during layer building because of the stochastic arrangement of the deposited powder on the bed and the continuous fluctuation of laser-powder interaction, respectively [6]. In addition, the quantity of building conditions renders the process of clarifying the building phenomena difficult.

The principal parameters for the laser scan strategy in PBF-LB/M are the laser power, laser scan speed [7], beam diameter [8], and powder layer thickness [9], which are used to calculate the specific energy density. Moreover, these process parameters change the microstructure and mechanical properties of the built parts [10]. In addition, various factors, such as hatching pitch and preheating temperature, are intricately involved.

Visualisation of the laser irradiation area appears to be promising as an effective means of clarifying the building phenomenon. This enables an understanding of the ejection phenomena of spatter particles and metal vapour jets from the melt pool during laser irradiation. Spatter particles deteriorate the surface characteristics and directly affect the quality of the built parts [11]. In addition, when large spatter particles are embedded in the component, the mechanical properties deteriorate [12]. Further, ejected fine particles in metal

Kotaro Tsubouchi
k.tsubouchi@stu.kanazawa-u.ac.jp

[1] Graduate School of Natural Science and Technology, Kanazawa University, Kakuma-machi, Kanazawa, Ishikawa 920-1192, Japan
[2] Advanced Manufacturing Technology Institute (AMTI), Kanazawa University, Kakuma-machi, Kanazawa, Ishikawa 920-1192, Japan
[3] Daido Steel Co., Ltd., Higashisakura 1-chome 1-10, Higashi, Nagoya, Aichi 461-8581, Japan

vapour jets cause beam ejection and absorption [13], while reduced beam quality causes ball effects on the surface of the built structure, deteriorating its properties as well [14]. Studies on laser welding have shown that the penetration depth becomes shallower owing to metal vapour jets [15]. Therefore, understanding the influence of process parameters on the ejecting phenomena of spatter particles and metal vapour jets is crucial. It has been revealed that these ejecting phenomena depend on major process parameters such as laser power and laser scan speed [16]. Further, atmospheric pressure has been proven to be one of the parameters affecting spattering phenomena [17].

However, the laser incident angle is also an important process parameter that changes depending on the building position in the PBF-LB/M machine in commercial AM equipment. Previous studies have shown the microstructure changes depending on the laser incident angle do not influence the mechanical properties, and an inclined laser beam reduces the specific energy of the irradiated area and increases the surface roughness [18]. However, the effect of the laser incident angle on the ejecting phenomenon is unclear. In addition, these studies targeted the current PBF-LB/M machine, and thus, the range of investigations of the laser incident angle must be expanded to meet the demand for larger machine sizes in the future.

Therefore, in this study, the melt pool in the single-track formation during the PBF-LB/M process was visualised using a high-speed camera, and the effect of the laser incident angle on the ejection behaviour of the spatter particles formed around the laser irradiation area was investigated. The cross-section of the single-track structure was observed through an optical microscope, and the melt pool was evaluated to reveal the thermal aspects during the PBF-LB/M process. However, pores remaining in the parts fabricated by the PBF-LB/M process are detrimental to the fatigue properties [19]. Consequently, the pores formed inside the single-track structure and the keyhole shape at the end point were investigated using X-ray computed tomography (CT). Thus, the above ejecting phenomena, alloyed area size, pore formation, and keyhole shape were comprehensively considered, and subsequently, the melt pool morphology during laser irradiation was inferred.

## 2. Materials and methods

A schematic of the experimental setup is shown in Fig. 1. The experiment was performed using a simplified form of the PBF-LB/M equipment composed of a building platform, a continuous-wave Yb fibre laser with Gaussian relative intensity (IPG Photonics Co., Ltd.: YLR - 300 - AC - Y11), a high-speed camera with a pixel matrix of 512×384 at a frame rate of 30000 fps (Photron Co., Ltd.: Fastcam Mini AX200), and a linear stage (GHC Hillstome Co., Ltd.: GHR25). Further, quartz glass windows

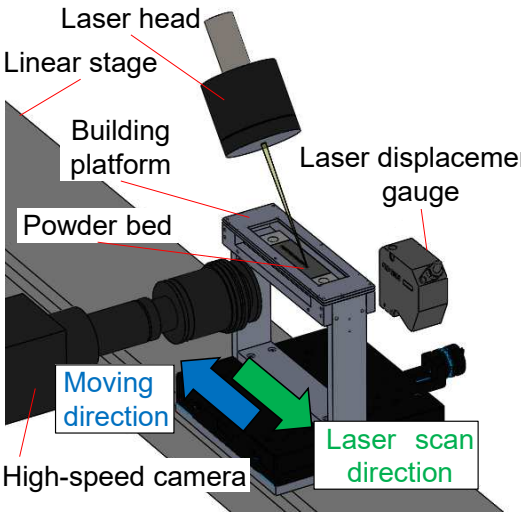


**Fig. 1** Experimental setup

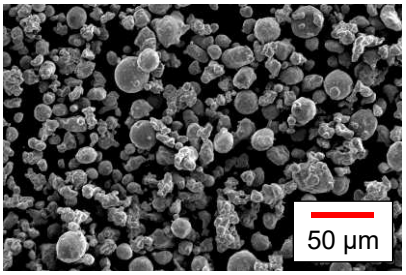


**Fig. 2** SEM image of metal powder

were provided on the upper and side surfaces of the building platform for the irradiation of the laser beam from the upper surface and the observation of metal powder morphology from the side surface, respectively. The oxygen level inside the building platform was maintained at 0.1 %, owing to filling with nitrogen gas, and controlled using an oximeter (Toray Engineering Co., Ltd: RF - 400). The Yb: fibre laser was focused onto a powder bed using a condenser with a focal length of 250 mm (Sigma Koki Co., Ltd.: SLSQ - 25–250P). Further, a high-speed camera was set perpendicular to the laser irradiation direction to observe the laser-irradiated area on the powder bed at the same height via the side quartz window. An optical filter (Sigma Koki Co., Ltd.: YL - 500P - Y1) was used to protect the image sensor of the high-speed camera from the scattered laser beam.

A scanning electron microscope (SEM) image of the metal powder used in the experiment is shown in Fig. 2, and the powder composition is shown in Table 1. The metal powder supplied was maraging steel with particle diameter in the range of 21.0 - 52.3 µm (D10 - D90), and average diameter of 33.3 µm (D50). In addition, an alloy tool steel (AISI: H13) with a thickness of 10 mm was prepared as the building substrate. The surface was sand-blasted for improved wettability using a grain size distribution of 212–300 µm, and it had a surface roughness of *Ra* 2.6 µm [20]. The metal powder was deposited on the

substrate with a levelling blade, and the powder thickness was confirmed using a laser displacement gauge (Keyence Corp., LK - 080).

A schematic of the metal powder behaviour when the laser beam was irradiated onto the powder bed is shown in Fig. 3, and the experimental conditions are summarised in Table 2. When the laser beam is irradiated onto the powder bed, a metal vapour plume, a metal vapour jet, and a spatter particle are induced from the laser-irradiated area. The metal vapour plume is among the principal factors that act as a driving force for the ejection of spatter particles [21]. In addition, the spatter particles are categorised into droplet spatter and powder spatter particles [22]. The former referred to as "hot spatter particles" are ejected by the convection of melted metal powder and the metal vapour jets induced around the melt pool whereas latter referred "cold spatter particles" are metal powder itself that is ejected by the act of metal vapour plume and metal vapour jet around the melt pool [23]. Thus, hot spatter particles are in a molten state and emit light, whereas cold spatter particles are comprised metals that have not melted. Solid spatter particles do not influence the quality of the built parts [24]. In the experiment, hot spatter particles with a large initial velocity owing to the metal vapour jet and a linear trajectory were evaluated. When a single track was formed on the substrate, the laser-irradiated area was observed using a high-speed camera, and the influence of the laser incident angle $\theta$ and scan speed on the spatter particle aspects were investigated. The number of spatter particles was evaluated by counting the spatter particles ejected from the melt pool when a single track was formed per unit length. Subsequently, 40 spatter particles were randomly selected to evaluate the various spatter particle aspects, and the ejection angle $\varphi$ was defined as the angle between the substrate surface and the averaged direction of the spatter particles. The laser incident angle was varied from 50 to 130 ° in parallel to the laser scan direction, while the laser beam size on the powder bed where the laser beam intensity fell to $1/e^2$ times ranged from 0.10 × 0.10 to 0.10 × 0.13 mm. However, the enforced gas flow was not provided inside the building platform for the removal of spatter particles and metal vapour jets. Ejected spatter particles were traced considering their high-speed images, and the ejecting phenomena of spatter particles and metallic vapour jets were identified. In addition, the cross-sections of a single track were observed after etching with 3 % nital solution using an optical microscope (Keyence Co., Ltd.: VHX - 1000) to evaluate the alloyed area after melt pool solidification. The width and depth of the alloyed area where the material composition of the powder and the substrate that were mixed was defined as indicated in Fig. 4 [25]. Further, the alloyed area refers to the melt pool during laser irradiation. In addition, defects such as pores and dents that were formed inside the alloyed area

**Table 1** Chemical composition of powder (wt%)

| Ni | Co | Mo | Ti | Al | Cr | Mn |
|---|---|---|---|---|---|---|
| 17.9 | 9.1 | 5.1 | 0.7 | 0.11 | 0.1 | 0.07 |
| Si | O | N | C | P | S | Fe |
| 0.06 | 0.03 | 0.02 | 0.01 | 0.009 | 0.004 | Bal. |

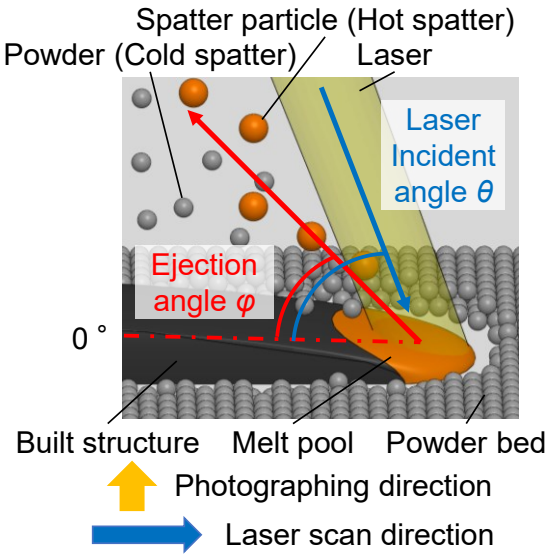


**Fig. 3** Schematic diagram of melting phenomenon

**Table 2** Experimental conditions

| | |
|---|---|
| **Laser irradiation** | |
| Laser type | Yb:fibre (CW) |
| Wavelength (nm) | 1070 |
| Laser spot diameter (mm) | 0.10 × 0.10 - 0.10 × 0.13 |
| Laser power (W) | 320 |
| Laser scan speed (mm/s) | 500, 700, 900 |
| Layer thickness (μm) | 50 |
| Laser incident angle (°) | 50 - 130 |
| **Atmosphere** | |
| Atmosphere of the chamber | $N_2$ |
| Oxygen concentration (%) | 0.1 |
| **Substrate** | |
| Material | AISI H13 |
| Thickness (mm) | 10 |
| **Powder** | |
| Material | maraging |
| Mean particle diameter (μm) | 33.3 |

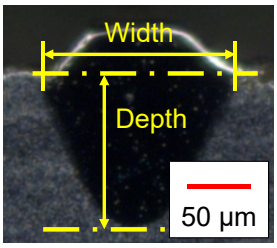


**Fig. 4** Definition of melt pool depth and width

were analysed using X-ray CT inspection equipment (Nikon Co., Ltd.: MCT225). The specimen for the analysis was prepared by cutting off the substrate, including a single track with a thickness of 600 μm, using a wire electric discharge machine (Sodick Co., Ltd.: AQ325L).

## 3. Results

### *3.1 Spattering phenomena of spatter particles and metal vapour jets*

Figure 5 compares the metal powder morphologies when the laser incident angles were 50 °, 90 °, and 130 °. A schematic is presented. The ejection of spatter particles and metal vapour jets was observed to be varying depending on the laser incident angle. When the laser incident angle was 50 °, as shown in Fig. 5a, the ejection angle of the spatter particles was small, and certain particles were ejected almost parallel to the substrate. However, an increase in the laser incident angle induced an upward ejection of spatter particles. The cold spatter particles were also ejected from the laser-irradiated area, and their characteristics were similar to those of the hot spatter particles. In addition, the cold spatter particles were kicked up according to the metallic vapour jets formed around the laser-irradiated area under laser incident angles of 50 ° and 90 °, respectively.

Figure 6 shows the variation in the ejection angle of the spatter particles as a function of the laser incident angle when the laser scan speed was varied from 500 to 900 mm/s. When the laser scan speed was 500 mm/s, the ejection angle was constant below the laser incident angle of 60 °. However, the ejection angle increased proportionally with an increase in the laser incident angle once it was over 60 °. Moreover, the increase in the ejection angle demonstrated the same tendency even when the laser scan speed was different. The threshold when the ejection angle was constant varied with the laser scan speed, and its value was 70 ° when the laser scan speed was 700 and 900 mm/s, respectively. In addition, the ejection angle increased as the laser scan speed increased.

Figure 7 shows the variation in the number of ejected spatter particles with the laser incident angle when the laser scan speed was varied from 500 to 900 mm/s. The number of ejected spatter particles increased as the laser incident angle increased. In addition, the decrease in the laser scan speed resulted in an increase in the ejection of spatter particles.

### *3.2 Spatter particle behaviour inside the optical path of laser beam*

Figure 8 shows the aspects of spatter particles inside the optical path of the laser beam starting from the beginning of spatter particle ejection from the melt pool ($t$ = 0 s) to $t$ = 733 μs at a laser scan speed of 500 mm/s and a laser incident angle of 70 °. These images were captured via a high-speed camera at a time interval of 67 μs. The

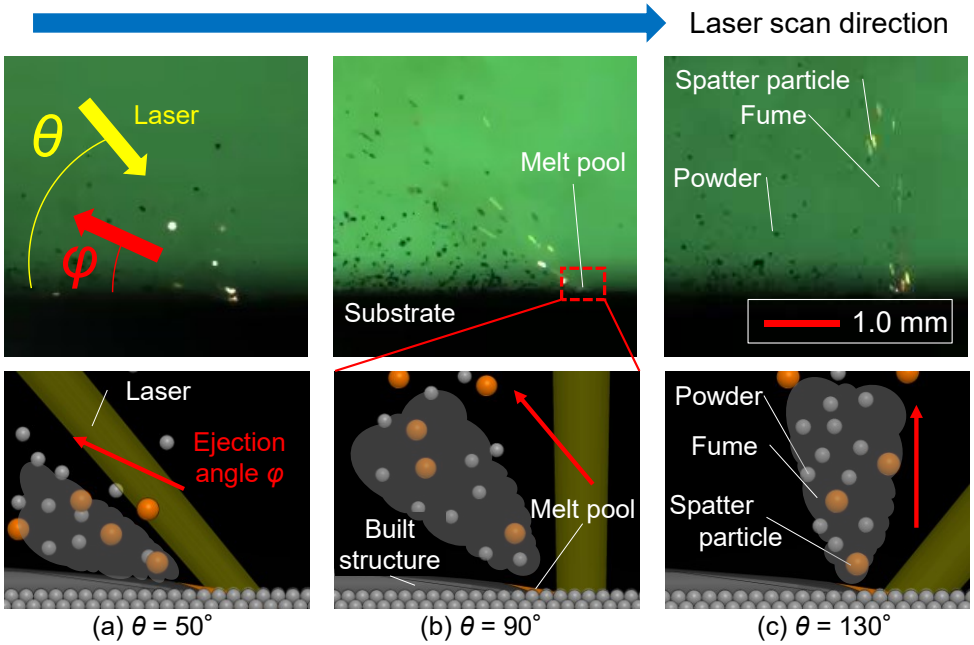


**Fig. 5** Comparison of spatter particle and metal vapour jets under the different laser incident angle $\theta$ at the laser scan speed 700 mm/s

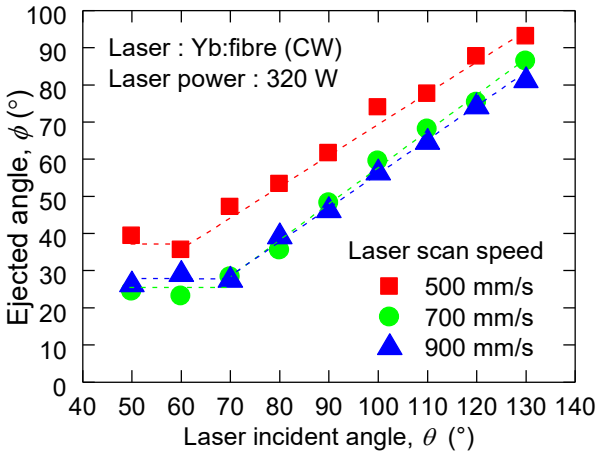


**Fig. 6** Variation of spatter particles direction ejected with laser incident angle

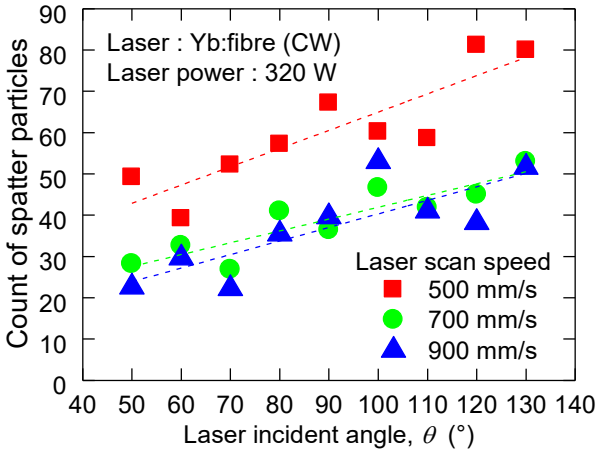


**Fig. 7** Variation of count of spatter particles per 1 mm irradiation length with laser incident angle

spatter particle ejected from melt pool, as depicted in Fig. 8a, and it intruded into the optical path of the laser beam, as shown in Fig. 8b. Furthermore, the metallic vapour jets that occurred from the surface of the spatter particle owing to the absorption of the laser beam, as shown in Fig. 8c. Subsequently, the intruded spatter particle was decelerated, as shown in Figs. 8d to 8f. Further, when the intruded time was 400 µs, as indicated in Fig. 8g, the spatter particle stopped moving owing to the interaction between the driving force of the spatter particle induced by the recoil pressure inside the melt pool at $t = 0$ s and the newly generated recoil pressure induced by the laser absorption of the spatter particle [26]. The maximum travel distance of spatter particle from the melt pool was 2.5 mm. Moreover, on attaining an intruded time of over 467 µs, as shown in Fig. 8h, the spatter particle changed the travelling direction and returned to the melt pool, as depicted in Figs. 8i–8l. The metallic vapour jets generated from the spatter particles decreased as the reversed distance increased.

Figure 9 shows the variation in the number of spatter particles that intruded into the optical path of the laser beam and resulted in a change in the ejection direction with the laser incident angle. The number of intruded spatter particles is related to the laser incident angle. When the laser incident angle was below 90 °, their numbers decreased with an increase in the laser incident angle, and no intruded spatter particles when the laser incident angle was over 90 °. In contrast, the spatter particle behaviour intruding into the optical path of the laser beam was not influenced by the laser scan speed.

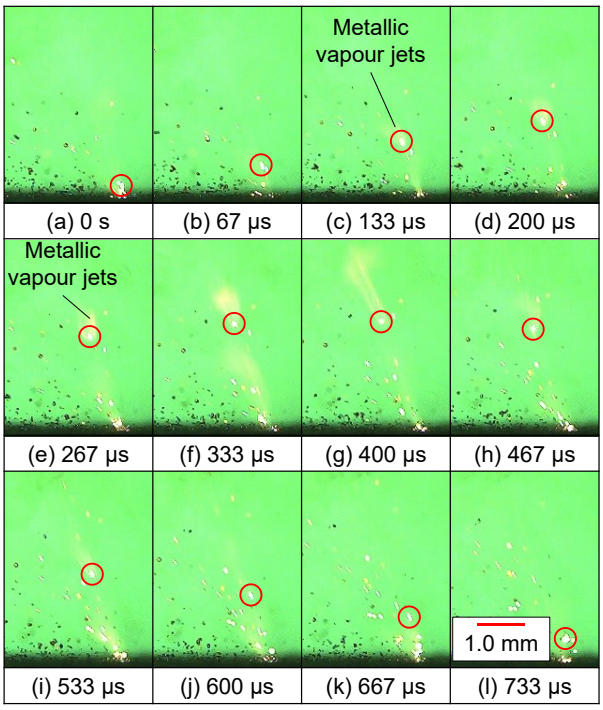


**Fig. 8** High-speed images captured at 66.7 µs intervals at incident angle of 70 ° and laser scan speed of 500 mm/s

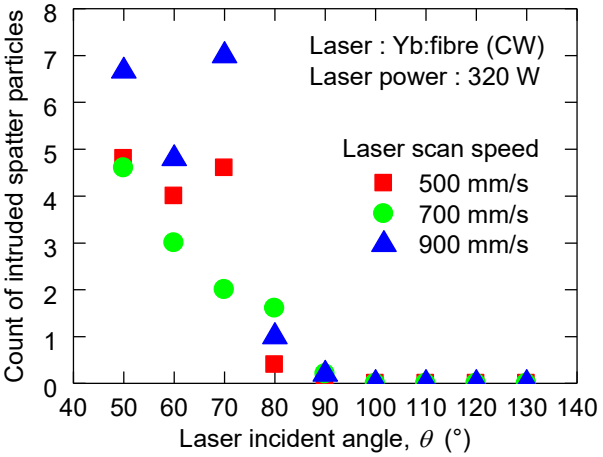


**Fig. 9** Variation of the intruded spatter particles per 10 mm irradiation length with the laser incident angle

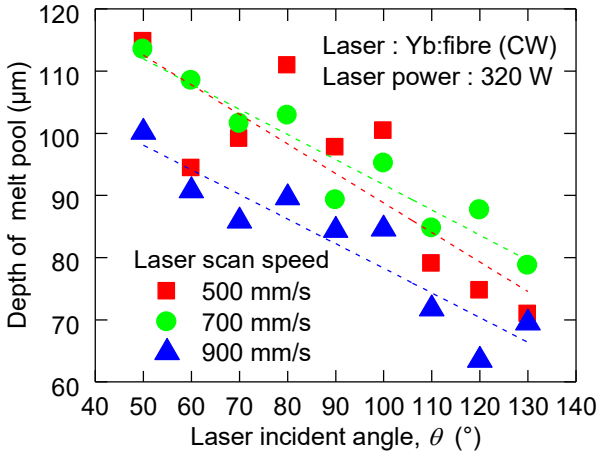


(a) Depth

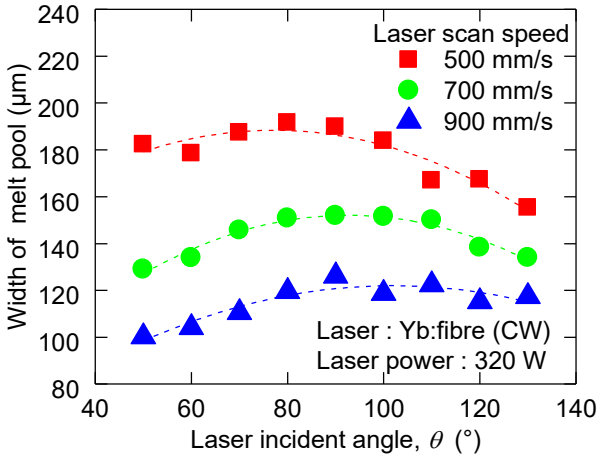


(b) Width

**Fig. 10** Relationship between the laser incidence angle $\theta$ and the alloyed area in the vertical cross-section of the single track

*3.3 Observation of alloyed area*

Figure 10 shows the variation in the alloyed area size with the laser incident angle. The depth alloyed area, as indicated in Fig. 10a, decreased with an increase in the laser incident angle. The depth at the angle of 130 ° was 70 μm, which was 1.4 times smaller than that at 50 ° at a laser scan speed of 900 mm/s. In addition, the depth increased with a decrease in the laser scan speed. However, for a laser scan speed further reduced from 700 mm/s to 500 mm/s, the value was decreased on average. Moreover, the melt pool width was the maximum value when the incidence angle was 90 ° owing to the change in the laser morphology at the powder bed, as shown in Fig. 10b. However, on increasing the laser scan speed the width at the same laser incident angle was reduced.

*3.4 Defect formation aspects inside the alloyed area*

Figure 11 compares the locations of the pores formed inside the alloyed area when the laser incident angle was different. For laser incident angle of 130 °, many pores

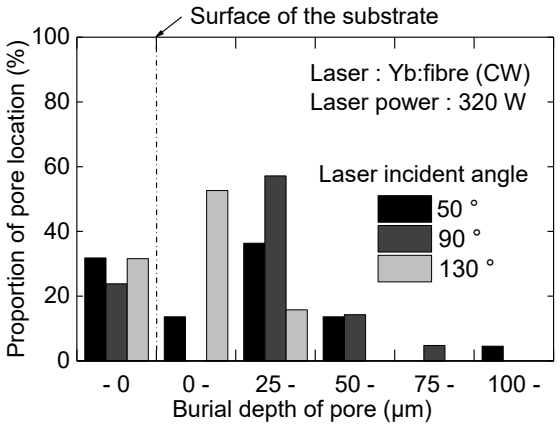


**Fig. 11** Distribution of burial depth of pores in the single track at the laser scan speed 700 mm/s

were formed near the substrate surface, although none were formed at depths greater than 50 μm. In contrast, the location of the pores was deep when the laser incident angle was 50 °.

Figure 12 compares the CT images at the final edge of a single track parallel to the laser scan direction. The depression morphology varied with the laser incident angle. For a laser incident angle of 50 °, a steep front wall was formed, and the depth of the depression was 63 μm. In contrast, a larger laser incident angle produced a shallower concavity with a gently sloping front wall, with a depth of 47 μm at 90 ° and 26 μm at 130 °.

## 4. Discussion

*4.1 Influence of laser incident angle on melt pool*

It was reported that the formation of the melt pool was divided into heat conduction and keyhole modes according to the input energy to the powder surface [27], and a melt pool with a depth greater than half the width was considered a keyhole [28]. Thus, considering this definition, each melting mode in this study was a keyhole mode under all conditions. A depression is formed under the melt pool during the PBF-LB/M processes under such conditions, and its shape is influenced by the input energy determined by the laser scan speed and power [29]. Moreover, depression affects the driving force of the melt pool and causes different heat convection in the melt pool [30]. As shown in Fig. 10, the melt pool became deeper and wider when the laser scan speed decreased. Further, the depression is continuously formed under the melt pool and is closed when the laser beam passes away from the melt pool. The protrusion at the edge of the depression front was believed to be a semi-molten particle before decay at a laser incident angle of 50 °, as shown in Fig. 12a [26]. Thus, observing the depression at the melt pool by dynamic observation during the laser beam irradiation was difficult, and the visualisation of depression was limited to methods using X-ray CT equipment [31]. However, the observation of a single track at the final edge enabled

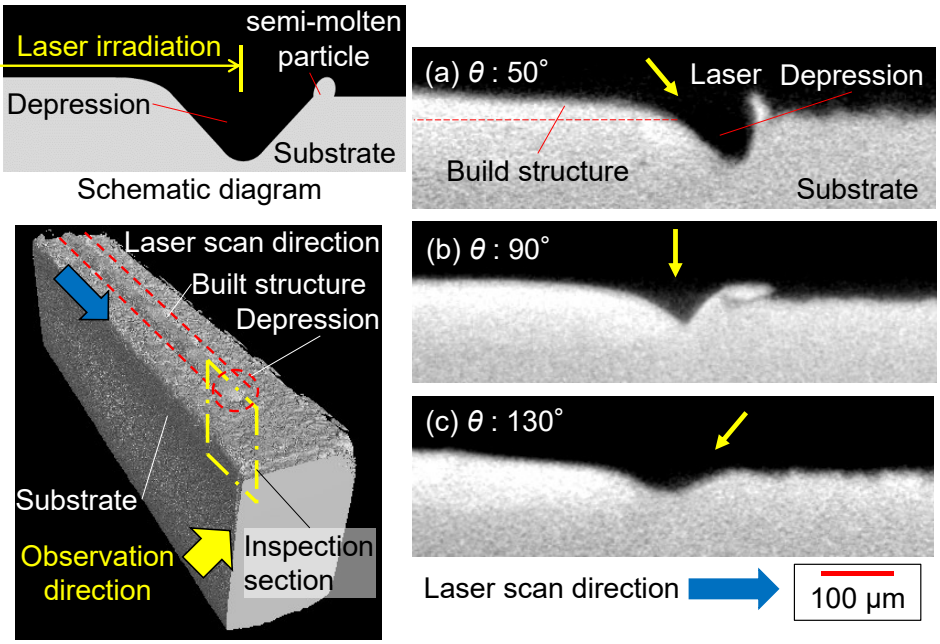


**Fig. 12** CT images of keyhole formed at the end of the single track at the laser scan speed 700 mm/s

the estimation of depression due to the maintenance of the melt pool morphology. The X-ray CT images at the final edge of a single track, as indicated in Fig. 12, showed that the depression, along with a smaller laser incident angle, was formed with a deep and steep front wall. In addition, as shown in Fig. 10a, the melt-pool depth increased as the laser incident angle was small. The width of the melt pool, as shown in Fig. 10b changed differently from the depth with the incident angle and reached its maximum value at an incident angle of 90 °. However, the width of the melt pool was primarily affected by the decrease in input energy owing to the increase in the spot long axis with the laser tilt. Thus, these results indicate that the melt pool morphology is affected not only by the laser scan speed and laser power, but also by the laser incident angle.

*4.2 Influence of laser incident angle on spatter particles behaviour*

Spatter particles ejected from the laser-irradiated area are among the principal factors that affect the building aspects during the PBF-LB/M processes. In the experiment, the effects of the laser incident angle during the PBF-LB/M processes on the metal powder morphology were experimentally investigated, and the interaction between the process parameters and the spatter particle behaviour was evaluated. A previous study revealed that metal vapour jets were ejected according to the depression morphology [32]. In addition, Cunningham et al. [31] concluded that the metal vapour jets were ejected parallel to the depression at a slow laser scan speed and high laser power and were ejected perpendicular to the front wall of the depression at a high laser scan speed and low input energy according to the keyhole morphology. Moreover, the ejection angle of the spatter particles, as indicated in Fig. 6, is related to both the laser scan speed and incident angle. For a small laser incident angle, the ejection angle of the spatter particles was small, and its aspects were directional with respect to the laser scan direction. Further, the depression morphology is determined via the laser incident angle, as described in 4.1 section, and the ejection angle of the spatter particles was equal to the vertical direction of the front wall in the depression shown in Fig. 12. Therefore, the ejection aspects of spatter particles were influenced by the laser incident angle and indirectly related to the depression morphology. Moreover, when the laser scan speed was 700 m/s and the laser incident angle was less than 70°, the spatter ejection angle was constant. The vertical direction of the front wall of the depression almost coincides with the substrate surface, thus it was considered that the ejection of the metal vapour jets and spatter particles was restricted by the building substrate, as shown in Fig. 5a.

In addition, Kawahito et al. [33] reported that the number of spatter particles in laser welding was reduced when the laser incident angle was less than 90 ° because of the change in the melt pool morphology. In this study, the number of spatter particles ejected decreased with decreasing laser incident angle, as shown in Fig. 7, which is evidence of the change in the melt pool morphology. Thus, the decrease in the laser incident angle was effective for the reduction of spatter particle formation in the PBF-LB/M processes.

*4.3 Influence of laser incident angle on laser obstructing*

The ejected spatter particles were observed to intrude into the optical path of the laser beam, as shown in Fig. 8.

As shown in Fig. 9, the number of intruded spatter particles decreased with a decrease in the laser incident angle, although the spatter particles did not intrude into the laser optical path when the laser incident angle was above 90 °. Further, the ejection of the spatter particles was restricted by the substrate when the incident angle was small, as shown in Fig. 5a, and they entered the laser optical path more easily than in Fig. 5b and c.

The dynamic observation of the laser-irradiated area indicated that the intruded spatter particles generated the metal vapour jets by absorbing the laser beam, resulting in the obstruction of the laser beam reaching the powder surface. It has been reported that fine particles (metal vapour jets) are generated when the plasma atom collides with each other [14], and the metal vapour jets generated from the laser-irradiated area absorbed 4.3 % of the fibre laser beam [34]. Therefore, it is necessary to establish a laser scan strategy wherein the spatter particles and metal vapour jets do not intrude into the laser optical path. In commercial PBF-LB/M equipment, the inert gas generally circulates inside the building chamber to eliminate the spatter particles and metal vapour jets from the optical path of the laser beam, and the ejection aspects of spatter particles affect their scatterable distance [35]. Therefore, the inert gas flow inside the building chamber must be considered in addition to the laser scan strategy, including the laser incident angle, to achieve a uniform building with quality assurance.

*4.4 Influence of laser incident angle on defects*

Depressions in the melt pool are also associated with the occurrence of pores. The maximum depth of the residual pores shown in Fig. 11 increased with decreasing laser incident angle. Zhao et al. [36] have shown via direct observation of the melt pool using megahertz X-ray imaging that pores were generated by the collapse of the melt pool and separation of the pointed end. In addition, Ng et al. [37] reported that the formation of pores depended on the melt pool morphology and the driving forces that induced the control of their motion. The pores were solidified at a deep position under the condition of deep depression. Consequently, it is considered that the difference in the melt pool morphology depending on the laser incident angle affected the pore formation. Therefore, the laser incident angle was proven to be an important factor in determining the defects in the built part.

## 5. Conclusions

In this study, simplified PBF-LB/M equipment was utilised to build a single track to experimentally investigate the influence of the laser incident angle on the melt pool morphology and the spatter particle behaviour. The melt pool during the PBF-LB/M process was visualised using a high-speed camera, and the cross-section of the single track was observed using an optical microscope and X-ray CT equipment. The primary results obtained are as follows:

(1) The depression shape formed at the edge of a single track varied with the laser incident angle. The evaluation of the depressions suggested that the melt pool morphology changed with the laser incident angle. Thus, the ejection aspects of spatter particles, melt pool morphology, and pore formation were found to be related to depression in the melt pool.
(2) The ejection aspects of the spatter particles varied with the laser incident angle, and the ejection angle decreased with decreasing laser incident angle. Further, the ejection angle of the spatter particles coincided with the vertical direction of the front wall of the depression. For incident angle less than 70°, the spatter particle ejection was restricted by the substrate.
(3) Spatter particles entering the laser optical path and obstructing the irradiation were generated owing to the restriction of ejection by the substrate.
(4) Pores remained at deeper positions with decreasing incident angle, and they were related to the depth of the depression during the melt pool formation.

In the commercial PBF-LB/M equipment, the inert gas circulates inside the building chamber to eliminate the spatter particles and metal vapour jets from the optical path of the laser beam, and the galvano mirror is placed above the centre position of the building platform to reach the laser beam at each position. Consequently, the laser incident angle at the building platform varies with the equipment configuration, and the building aspect differs according to its configuration. Therefore, to establish a laser scan strategy for a high-quality building, the evaluation of melt pool behaviour using commercial PBF-LB/M equipment is needed in future work. The mechanical properties of the built structure were not evaluated in this study. An investigation of the effect of the laser incident angle on the quality of the product, such as tensile strength and hardness, is required.

**Authors' contributions** TK: Conducted the in-process monitoring, evaluated the obtained data, organised all data, and wrote the manuscript. FT: Proposed the experiment and evaluation method to reveal the effect of the laser incident angle on melting phenomena, conducted the In-process monitoring, and evaluated the obtained data. YM: Evaluated the cross-section of a single track using an optical microscope. EA: Evaluated depression at the final edge of a single track using X-ray CT. YS, OM and SK: Supplied the metal powder and evaluated the obtained data.

**Data availability** Not applicable.

**Code availability** Not applicable.

## Declarations

**Ethics approval** Not applicable.

**Consent to participate** Not applicable.

**Consent for publication** Not applicable.

**Conflict of interest** The authors declare no competing interest.

## References


1. ASTM F2792-10[e1] (2012) Standard terminology for additive manufacturing technologies, Annual book of ASTM Standard, ASTM International, Pennsylvania 671-673.
2. Vayre B, Vignat F, Villeneuve F (2012) Designing for Additive Manufacturing. Proc CIRP 3:632-637. https://doi.org/10.1016/j.procir.2012.07.108
3. Plessis AD, Yadroitsava I, Yadroitsav I (2018) Ti6Al4V lightweight lattice structures manufactured by laser powder bed fusion for load-bearing applications. Opt Laser Technol 108:521-528. https://doi.org/10.1016/j.optlastec.2018.07.050
4. Tan C, Wang D, Ma W, Chan Y, Chen S, Yang Y, Zhou K (2020) Design and additive manufacturing of novel conformal cooling molds. Mater Des 196:109147. https://doi.org/10.1016/j.matdes.2020.109147
5. Nadimpalli VK, Dahmen T, Valente EH, Mohanty S, Pedersen DB (2019) Multi-material additive manufacturing of steels using laser powder bed fusion. Eur Soc Precis Eng Nanotechnol:240-243.
6. Bayat M, Thanki A, Mohanty S, Witvrouw A, Yang S, Thorborg J, Tiedje NS, Hattel JH (2019) Keyhole-induced porosities in Laser-based Powder Bed Fusion (L-PBF) of Ti6Al4V: High-fidelity modelling and experimental validation. Addit Manuf 30: 100835. https://doi.org/10.1016/j.addma.2019.100835
7. Bertoli US, Wolfer AJ, Matthews MJ, Delplanque JR, Schoenung JM (2017) On the limitations of Volumetric Energy Density as a design parameter for Selective Laser Melting. Mater Des 113 (5):331-340. https://doi.org/10.1016/j.matdes.2016.10.037
8. Metelkova J, Kinds Y, Kempen K, Formanoir C, Witvrouw A, Hooreweder BV (2018) On the influence of la-ser defocusing in Selective Laser Melting of 316L. Addit Manuf 23:161-169. https://doi.org/10.1016/j.addma.2018.08.006
9. Qiu C, Panwisawas C, Ward M, Basoalto HC, Brooks JW, Attallah MM (2015) On the role of melt flow into the surface structure and porosity development during selective laser melting. Acta Mater 96 (1):72-79. https://doi.org/10.1016/j.actamat.2015.06.004
10. Gu DD, Meiners W, Wissenbach K, Poprawe R (2012) Laser additive manufacturing of metallic components: materials, processes and mechanisms. Int Mater Rev 57 (3):133-164. https://doi.org/10.1179/1743280411Y.0000000014
11. Sato N, Seto N, Shimizu T, Nakano S (2017) Real-time Observation of Melting Behaviour in Selective Laser Melting of Metals. Mater Japan 56 (12):695–698.
12. Wang D, Yang Y, Liu R, Xiao D, Sun J (2013) Study on the designing rules and processability of porous structure based on selective laser melting (SLM). J Mater Process Technol 213 10:1734–1742. https://doi.org/10.1016/j.jmatprotec.2013.05.001
13. Arai T (2013) Fundamental Engineering Science for Laser Materials Processing. Maruzen Publishing Co.,Ltd., Tokyo
14. Ladewig A, Schlick G, Fisser M, Schulze V, Glatzel U (2016) Influence of the shielding gas flow on the removal of process by-products in the selective laser melting process. Addit Manuf 10:1-9. https://doi.org/10.1016/j.addma.2016.01.004
15. Miyazaki Y, Katayama S (2013) Influence of Laser-Induced Plume on Penetration in Laser Welding, Q J Jpn Weld Soc 31 (2):119–125. https://doi.org/10.2207/qjjws.31.119
16. Bidare P, Bitharas I, Ward RM, Attallah MM, Moore AJ (2018) Fluid and particle dynamics in laser powder bed fusion. Acta Mater 142 (1):107-120. https://doi.org/10.1016/j.actamat.2017.09.051
17. Matthews MJ, Guss G, Khairallah SA, Rubenchik AM, Depond PJ, King WE (2016) Denudation of metal powder layers in laser powder bed fusion processes. Acta Mater 114 (1):33-42. https://doi.org/10.1016/j.actamat.2016.05.017
18. Sendino S, Gardon M, Lartategui F, Martinez S, Lamikiz A (2020) The Effect of the Laser Incidence Angle in the Surface of L-PBF Processed Parts. Coat 10 (11):1024. https://doi.org/10.3390/coatings10111024
19. Leuders S, Thöne, M, Riemer A, Niendorf T, Tröster T, Richard HA, Maier HJ (2013) On the mechanical behaviour of titanium alloy TiAl6V4 manufactured by selective laser melting: Fatigue resistance and crack growth performance. Int J Fatigue 48:300–307. https://doi.org/10.1016/j.ijfatigue.2012.11.011
20. Furumoto T, Egashira K, Oishi K, Abe S, Yamaguchi M, Hashimoto Y, Koyano T, Hosokawa A (2021) Experimental investigation into the spatter particle behaviour of maraging steel during selective laser melting. J Adv Mech Des Syst Manuf 15(4):JAMSDM0039. https://doi.org/10.1299/jamdsm.2021jamdsm0039

21. Guo Q, Zhao C, Escano LI, Young Z, Xiong L, Fezzaa K, Everhart W, Brown B, Sun T, Chen L (2018) Transient dynamics of powder spattering in laser powder bed fusion additive manufacturing process revealed by in-situ high-speed high-energy x-ray imaging. Acta Mater 151:169–180. https://doi.org/10.1016/j.actamat.2018.03.036
22. Liu Y, Yang Y, Mai S, Wang D, Song C (2015) Investigation into spatter behaviour during selective laser melting of AISI 316L stainless steel powder. Mater Des 87(15):797–806. https://doi.org/10.1016/j.matdes.2015.08.086
23. Andani MT, Dehghani R, Ravari MRK, Mirzaeifar R, Ni J (2017) Spatter formation in selective laser melting process using multi-laser technology. Mater Des 131(5):460-469. https://doi.org/10.1016/j.matdes.2017.06.040
24. Wang D, Wu S, Fu F, Mai S, Yang Y, Liu Y, Song C (2017) Mechanisms and characteristics of spatter generation in SLM processing and its effect on the properties. Mater Des 117(5):121-130. https://doi.org/10.1016/j.matdes.2016.12.060
25. Furumoto T, Ueda T, Kobayashi N, Yassin A, Hosokawa A, Abe S (2009) Study on laser consol-idation of metal powder with Yb:fiber laser—Evaluation of line consolidation structure. J Mater Process Technol 209(18-19):5973-5980. https://doi.org/10.1016/j.jmatprotec.2009.07.017
26. Khairallah SA, Anderson AT, Rubenchik A, King WE (2016) Laser powder-bed fusion additive manufacturing: Physics of complex melt flow and formation mechanisms of pores, spatter, and denudation zones. Acta Mater 108(15):36-45. https://doi.org/10.1016/j.actamat.2016.02.014
27. Steen WM, Mazumder J (2010) Laser material processing,4th edn. Springer, London https://doi.org/10.1007/978-1-84996-062-5
28. King WE, Barth HD, Castillo VM, Gallegos GF, Gibbs JW, Hahn DE, Kamath C, Rubenchik AM (2014) Observation of keyhole-mode laser melting in laser powder-bed fusion additive manufacturing. J Mater Process Technol 214(12):2915–2925. https://doi.org/10.1016/j.jmatprotec.2014.06.005
29. Ly S, Rubenchik AM, Khairallah SA, Guss G, Matthews MJ (2017) Metal vapor micro-jet controls material redistribution in laser powder bed fusion additive manufacturing. Sci Rep 7:4085 https://doi.org/10.1038/s41598-017-04237-z
30. Gao M, Kawahito Y, Kajii S (2017) Observation and understanding in laserwelding of pure titanium at subatmospheric pressure. Opt Express 25(12):13539-13548 https://doi.org/10.1364/OE.25.013539
31. Cunningham R, Zhao C, Parab N, Kantzos C, Pauza J, Fezzaa K, Sun T, Rollett AD (2019) Keyhole threshold and morphology in laser melting revealed by ultra-high-speed x-ray imaging distribution on the powder bed during selective laser melting. Science 363(6429):849-852. https://doi.org/10.1126/science.aav4687
32. Young ZA, Guo Q, Parab ND, Zhao C, Qu M, Escano LI, Fezzaa K, Everhart W, Sun T, Chen L (2020) Types of spatter and their features and formation mechanisms in laser powder bed fusion additive manufacturing process. Addit Manuf 36:101438. https://doi.org/10.1016/j.addma.2020.101438
33. Kawahito Y, Nakada K, Uemura Y, Mizutani M, Nishimoto K, Kawakami H, Katayama S (2018) Relationship between melt flows based on three-dimensional X-ray transmission in-situ observation and spatter reduction by angle of incidence and defocus distancing distance in high-power laser welding of stainless steel. Weld Int 32(7):485-496. https://doi.org/10.1080/01431161.2017.1346887
34. Kawahito Y, Kinoshita K, Matsumoto N, Mizutani M, Katayama S (2007) Interaction between laser beam and plasma/plume induced in welding of stainless steel with ultra-high power density fiber laser. Q J Jpn Weld Soc 25 (3):461-467. https://doi.org/10.2207/qjjws.25.461
35. Anwar AB, Pham QC (2018) Study of the spatter distribution on the powder bed during selective laser melting. Addit Manuf 22:86-97. https://doi.org/10.1016/j.addma.2018.04.036
36. Zhao C, Parab ND, Li X, Fezzaa K, Tan W, Rollett AD, Sun T (2020) Critical instability at moving keyhole tip generates porosity in laser melting. Science 370(6520):1080-1086. https://doi.org/10.1126/science.abd1587
37. Ng GKL, Jarfors AEW, Bi G, Zheng HY (2009) Porosity formation and gas bubble retention in laser metal deposition. Appl Phys A 97:641. https://doi.org/10.1007/s00339-009-5266